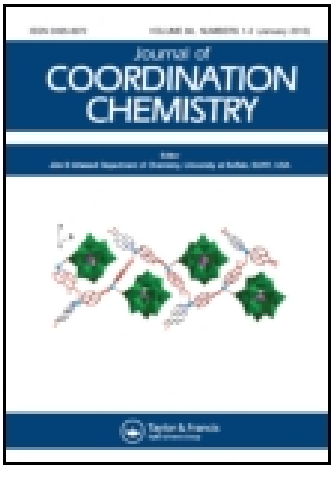

Journal of Coordination Chemistry
Publication details, including instructions for authors and subscription information:
http://www.tandfonline.com/loi/gcoo20

Mono and dinuclear copper(II) naproxenato complexes containing 3-picoline and 4-picoline: synthesis, structure, properties, catechol oxidase, and antimicrobial activities

Sema Caglar[a], Ekrem Adiguzel[a], Bahtiyar Sariboga[b], Ersin Temel[c] & Orhan Buyukgungor[c]

[a] Faculty of Arts and Sciences, Department of Chemistry, Erzincan University, Erzincan, Turkey

[b] School of Health, Sinop University, Sinop, Turkey

[c] Faculty of Arts and Sciences, Department of Physics, Ondokuz Mayis University, Samsun, Turkey

Accepted author version posted online: 05 Feb 2014.Published online: 05 Mar 2014.

To cite this article: Sema Caglar, Ekrem Adiguzel, Bahtiyar Sariboga, Ersin Temel & Orhan Buyukgungor (2014) Mono and dinuclear copper(II) naproxenato complexes containing 3-picoline and 4-picoline: synthesis, structure, properties, catechol oxidase, and antimicrobial activities, Journal of Coordination Chemistry, 67:4, 670-683, DOI: 10.1080/00958972.2014.891198

To link to this article: http://dx.doi.org/10.1080/00958972.2014.891198

Journal of Coordination Chemistry, 2014
Vol. 67, No. 4, 670–683, http://dx.doi.org/10.1080/00958972.2014.891198

Mono and dinuclear copper(II) naproxenato complexes containing 3-picoline and 4-picoline: synthesis, structure, properties, catechol oxidase, and antimicrobial activities

SEMA CAGLAR*†, EKREM ADIGUZEL†, BAHTIYAR SARIBOGA‡, ERSIN TEMEL§ and ORHAN BUYUKGUNGOR§

†Faculty of Arts and Sciences, Department of Chemistry, Erzincan University, Erzincan, Turkey
‡School of Health, Sinop University, Sinop, Turkey
§Faculty of Arts and Sciences, Department of Physics, Ondokuz Mayis University, Samsun, Turkey

(*Received 22 October 2013; accepted 14 January 2014*)

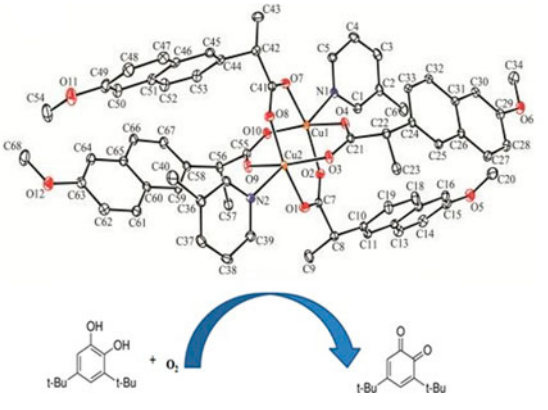

Mononuclear and dinuclear copper(II) complexes $[Cu_2(\mu\text{-nap})_4(3\text{-pic})_2]$ (**1**) and $[Cu(nap)_2(H_2O)(4\text{-pic})_2]$ (**2**) have been synthesized in the presence of 3-picoline and 4-picoline. Two complexes were characterized by FT-IR, UV–vis spectroscopic methods and their thermal stabilities were determined by TG/DTA/DTG techniques. The crystal structures of **1** and **2** were established by X-ray analysis. X-ray structure analysis has shown that copper(II) has a distorted square-pyramidal geometry. Naproxenate is a bridging ligand in **1** and monodentate in **2**. Two complexes have shown catalytic activity on oxidation of 3,5-di-*tert*-butylcatechol to 3,5-di-*tert*-butylquinone exhibiting saturation kinetics at high substrate concentrations. The complexes were also screened for antimicrobial activity against pathogenic bacteria and fungi. The complexes exhibited antimicrobial activity against *Entrococcus faecalis* and *Candida albicans*.

Keywords: Naproxen; Catechol oxidation; Antimicrobial activity; Copper(II) complex

*Corresponding author. Email: scaglar@erzincan.edu.tr

1. Introduction

Nonsteroidal antiinflammatory drugs (NSAIDs) demonstrate analgesic, antiinflammatory, and antipyretic properties and are used for pain and inflammation. NSAIDs have a role on the activity of certain antitumor drugs [1, 2]. Several studies have shown that the influences of NSAIDs are essentially based on inhibition of cyclooxygenase. Cyclooxygenase converts the arachidonic acid into prostaglandins, prostacyclin, and thromboxane [3, 4], but the mechanisms have not been clearly explained. Salicylate derivatives, phenylalkanoic acids, oxicams, anthranilic acids, sulfonamides, and furanones are the basic forms of NSAIDs [5]. Naproxen (=Hnap), which relates to the NSAIDs group of phenylalkanoic acids, is (+)-6-methoxy-α-methyl-2-naphthalene acetic acid. In the literature, the crystal structures of metal complexes of naproxen, for example copper(II) [6–9], cobalt(II) [10], zinc(II) [11], cadmium(II) [12], and ruthenium(II, III) [2], have been reported. NSAIDs with copper(II) complexes have been studied because they are more active than their parent drugs [5, 13].

Copper(II) plays a role in differing biological processes such as electron transfer, oxidation, and dioxygen transport [14, 15] and varied enzymatic reactions, such as catechol oxidase [16–26] activity. Catechol oxidase enzyme, which exists in nature in plants, insects, and crustaceans, plays an important role in disease resistance in higher plants [27]. The catechol oxidase reaction is of importance and used in medical diagnosis [28]. Catechol oxidaze catalyzes the two-electron oxidation of catechols in the presence of oxygen to the corresponding quinones [18]. Catalytic activity of complex for the oxidation of 3,5-di-*tert*-butylcatechol to the corresponding quinone in methanol has been studied by UV–Vis spectroscopy (figure 1). Several mononuclear and binuclear copper complexes with nitrogen and oxygen donors display major catecholase activity [21, 29–31]. The mechanism of catechol oxidation by the natural enzyme, as proposed by Krebs and co-authors, was studied [32].

In the current study, we report the synthesis, structural characterization, catechol oxidase, and antimicrobial activities of copper(II) complexes with naproxenate in the presence of 3-picoline (3-pic) and 4-picoline (4-pic) (figure 2).

2. Experimental setup

2.1. *Materials*

Naproxen and other chemicals and solvents used in this study were of high purity (Aldrich or Sigma chemicals) and were used without purification. Infrared spectra of the complexes were recorded with a Thermo Nicolet 6700 FT-IR spectrophotometer from 4000 to 450 cm^{-1} and at a resolution of 0.5 cm^{-1} by using KBr pellets. UV–vis spectra

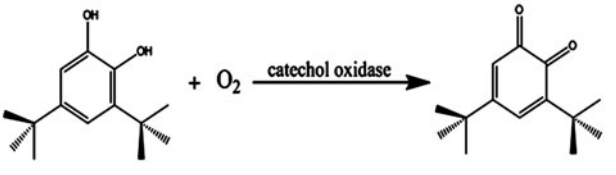

Figure 1. Oxidation of 3,5-di-*tert*-butylcatechol by **1** and **2**.

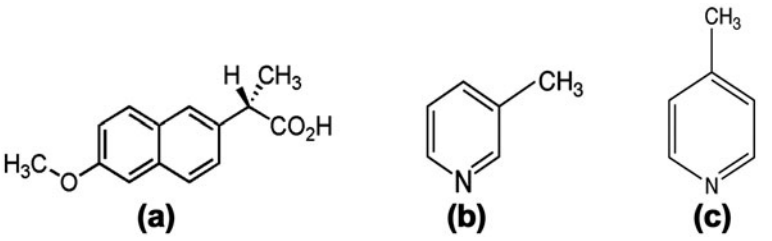

Figure 2. Molecular structure of naproxen (a), 3-picoline (b), and 4-picoline (c).

were recorded on a PG 80+ UV–vis spectrophotometer from 200 to 900 nm in methanol. C, H, and N elemental analyses were performed on a LECO CHNS-932 elemental analyzer. TG and DTA curves were scanned using a PRIS Diamond TG/DTG apparatus in static air (heating rate: 10 °C min^{-1}, platinum crucibles, mass ~10 mg, and temperature range: 30–1000 °C). The powder X-ray diffraction (PXRD) patterns of final solid products in thermal analysis studies were taken at ambient temperatures using a PANalytical Empyrean diffractometer using Ni-filtered CuK_α radiation (l = 1.54050 Å; 45 kV and 40 mA).

2.2. *Synthesis*

2.2.1. $[Cu_2(\mu\text{-nap})_4(3\text{-pic})_2]$ (1). Potassium hydroxide (0.4 mM, 22 mg) was added to a methanol solution (15 mL) of naproxen (0.4 mM, 92 mg) and the solution was stirred for 1 h at 50 °C. 3-pic (98 µL, 0.6 mM) was added into ethanol solution (10 mL) of $CuSO_4{\cdot}5H_2O$ (0.04 g, 0.2 mM) and stirred for 30 min. at 50 °C. Then, the first solution was added to the second solution. X-ray quality green crystals of $[Cu_2(\mu\text{-nap})_4(3\text{-pic})_2]$ were obtained by slow evaporation of the solution at room temperature within a few days. Yield: 80%; microanalytical data for $[C_{68}H_{66}N_2O_{12}Cu_2]$: Found: C, 66.48; H, 5.30; N, 2.21%; calcd: C, 66.32; H, 5.34; N, 2.28%.

2.2.2. $[Cu(nap)_2(H_2O)(4\text{-pic})_2]$ (2). Complex **2** was prepared in a similar way to **1** with the use of 4-pic (98 µL, 0.6 mM) instead of 3-pic. X-ray quality blue crystals of $[Cu(nap)_2(H_2O)(4\text{-pic})_2]$ were obtained by slow evaporation of the solution at room temperature after one week. Yield: 85%; microanalytical data for $[C_{40}H_{42}N_2O_7Cu]$: Found: C, 66.12; H, 5.85; N, 3.88%; calcd: C, 66.09; H, 5.78; N, 3.85%.

2.3. *X-ray crystallography*

Diffraction measurements were performed at 296 K on a STOE IPDS II diffractometer using graphite monochromated Mo-Kα radiation. Crystals of $C_{68}H_{66}N_2O_{12}Cu_2$ and $C_{40}H_{42}N_2O_7Cu$ have approximate dimensions of 0.480 × 0.347 × 0.110 mm and 0.610 × 0.233 × 0.040 mm, respectively. A summary of the key crystallographic information is given in table 1. Data collection: Stoe X-AREA [33]. Cell refinement: Stoe X-AREA [33]. Data reduction: Stoe X-RED [33]. The structure was solved by direct methods using SHELXS-97 [34] and anisotropic displacement parameters were applied to nonhydrogen atoms in a full-matrix least-squares refinement based on F^2 using SHELXL-97 [34]. All hydrogens

Table 1. Crystal data and structure refinement parameters for **1** and **2**.

	1	**2**
Empirical formula	$C_{68}H_{66}N_2O_{12}Cu_2$	$C_{40}H_{42}N_2O_7Cu$
Formula weight	1230.31	726.30
Temperature (K)	296	296
Wavelength (Å)	0.71073	0.71073
Crystal system	Monoclinic	Monoclinic
Space group	*P21*	*P21*
Unit cell dimensions		
a (Å)	16.2796(4)	16.4555(14)
b (Å)	10.3629(4)	5.7365(3)
c (Å)	18.7360(5)	19.2458(15)
α (°)	90	90
β (°)	110.082(2)	101.461(7)
γ (°)	90	90
V (Å)^3	2968.66(16)	1780.5(2)
Z	4	2
Absorption coefficient (mm^{-1})	0.782	0.666
D_{calcd} (mg m^{-3})	1.3764(1)	1.355
Crystal size (mm)	0.480; 0.347; 0.110	0.610; 0.233; 0.040
Theta range for data collection (°)	1.43; 28.06	1.49; 28.07
Measured reflections	28588	14582
Independent reflections	9358	3411
Absorption correction	Integration[a]	Integration[a]
Refinement method	Full-matrix least-squares on F^2	Full-matrix least-squares on F^2
Final R indices [$F^2 > 2\sigma(F^2)$]	0.0537	0.0929
Goodness-of-fit on F^2	0.958	0.987

[a]Stoe and Cie (2002) [35].

attached to carbon were positioned geometrically and refined by a riding model assigning U_{iso} equal to 1.2 times that of attached atoms; remaining hydrogens were located from the Fourier difference map.

2.4. *Catechol oxidase activity*

The catalytic oxidation of 3,5-di-*tert*-butylcatechol ($DTBCH_2$) by copper complexes was evaluated in dioxygen-saturated methanol at room temperature. The reaction was monitored spectrophotometrically by choosing the strongest absorbance. Because 3,5-di-*tert*-butylquinone (3,5-DTBQ) is stable and has a strong absorption at 395 nm, the initial reaction rate was determined from the slope of the trace at 395 nm in the first 1 min. of the reaction. While the initial rate was being determined, different ratios of complex and substrate were studied. The minimum complex to substrate rate was 1 : 5 and the maximum complex to substrate rate was 1 : 50. K_m, V_{max}, and k_{cat} values were determined by Lineweaver–Burk plots and the Michaelis–Menten equation.

2.5. *Antimicrobial assays*

The potential antimicrobial effects of the Cu(II) complexes were investigated by microdilution method against five Gram-positive bacteria, *Bacillus cereus* (ATCC 7064), *Entrococcus faecalis* (ATCC 15753), *Listeria monocytogenes* (ATCC 19114), *Staphylococcus aureus* (ATCC 6538), and *Methicillin Resistant S. aureus* MRSA (ATCC 43300); three Gram-negative bacteria *Salmonella typhi* (CCM 5445), *Escherichia coli* (ATCC 35218), and

Pseudomonas aeruginosa (ATCC 27853); and one yeast *Candida albicans* (ATCC 10231). The complexes were dissolved in DMSO to a final concentration of 4096 μg mL^{-1} and then sterilized by filtration using 0.20 μm Millipore. Negative controls were prepared by using DMSO. Vancomycin, ciprofloxacin, and Amphotericine B were used as positive reference standards. The minimum inhibitor concentration (MIC, μg mL^{-1}) value was determined as the lowest concentration at which the growth of micro-organisms was not observed. All experiments were performed in duplicate and confirmed by three separate experiments. The antibacterial activity assays of all compounds were performed according to the Clinical and Laboratory Standards Institute protocols [35]. The antifungal activities of all compounds were evaluated according to the National Committee for Clinical Laboratory Standards [36]. The bacteria were incubated in Muller Hinton Broth (Oxoid) at 37 °C for 24 h. The yeast was incubated in RPMI-1640 medium (Biological Industries) at 35 °C for 48 h.

3. Results and discussion

3.1. *Crystal structure of 1*

The molecular structure of **1** is shown in figure 3 and selected bond distances and angles are listed in table 2. In $[Cu_2(\mu\text{-nap})_4(3\text{-pic})_2]$ (**1**), four deprotonated naproxenates (nap) are in bridging mode and nap ligands connect two adjacent copper(II) ions via eight carboxylate oxygens from four nap ligands.

Cu1(II) and Cu2(II) are five-coordinate with distorted square-pyramidal geometry, with both coppers surrounded by four nap ligands and one 3-picoline. The structural distortion index tau (τ) was calculated as 0.125 for Cu1 and 0.118 for Cu2, clearly suggesting a distorted square-pyramidal geometry for **1** ($\tau = a - b/60$, where a and b correspond to the two angles showing a tendency to linearity). The τ-values of square-based-pyramidal and trigonal-bipyramidal extremes are 0 and 1, respectively [37].

Intermolecular hydrogen bond between hydrogen of methoxy of nap and oxygen of methoxy of nap is given in table 3 (figure 4).

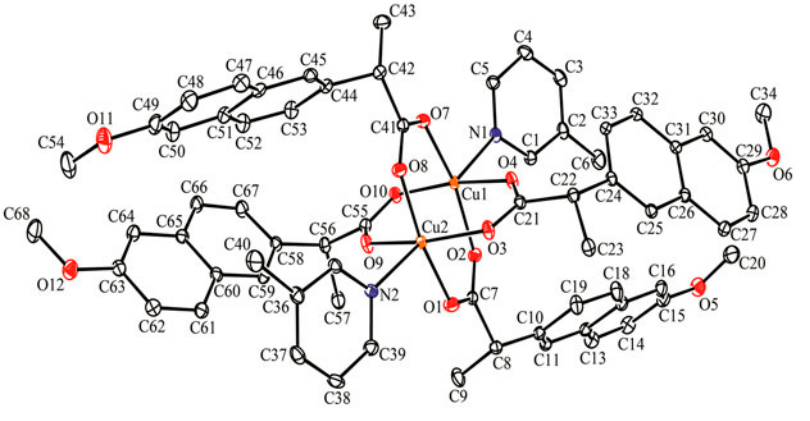

Figure 3. ORTEP III diagram and atom numbering scheme of **1**. Displacement ellipsoids are drawn at the 20% probability level.

Table 2. Selected bond distances (Å) and angles (°) for **1** and **2**.

1			
Cu1–N1	2.180(3)	Cu2–N2	2.164(3)
Cu1–O2	1.991(3)	Cu2–O1	1.951(3)
Cu1–O4	1.961(3)	Cu2–O3	1.996(3)
Cu1–O7	1.994(3)	Cu2–O8	1.935(3)
Cu1–O4	1.961(3)	Cu2–O9	2.028(3)
O4–Cu1–O10	170.36(11)	O8–Cu2–O1	168.89(11)
O4–Cu1–O2	88.09(12)	O8–Cu2–O3	88.73(13)
O2–Cu1–O10	87.30(12)	O1–Cu2–O3	86.67(14)
O4–Cu1–O7	91.36(13)	O8–Cu2–O9	92.65(13)
O7–Cu1–O10	90.57(13)	O1–Cu2–O9	88.61(14)
O7–Cu1–O2	162.86(10)	O3–Cu2–O9	161.79(10)
O7–Cu1–N1	86.60(10)	O8–Cu2–N2	94.08(11)
O10–Cu1–N1	102.52(10)	O9–Cu2–N2	87.82(10)
2			
Cu1–N1	2.062(9)	Cu1–O4	1.961(8)
Cu1–N2	2.017(8)	Cu1–O2	2.423(9)
Cu1–O1	2.002(8)		
O1–Cu1–N1	91.6(3)	N1–Cu1–N2	175.9(4)
O4–Cu1–N1	88.6(4)	O4–Cu1–O7	95.5(3)
O1–Cu1–N2	88.5(3)	O1–Cu1–O7	96.4(3)
O4–Cu1–N2	90.5(3)	O7–Cu1–N2	93.2(3)
O4–Cu1–O1	168.1(3)	O7–Cu1–N1	90.9(3)

Table 3. Hydrogen-bonding geometries for **1** and **2** (Å, °).

D–H···A	D–H	H···A	D···A	D–H···A
1				
C68–H68A···O11^{i}	0.96	2.51	3.464(6)	157
2				
O7–HB···O2	0.86	2.01(10)	2.665(12)	132(9)
O7–HA···O1^{ii}	0.86	2.33(8)	3.017(11)	139(10)
C7–H7···O4^{iii}	0.93	2.48	3.183(13)	132
C29–H29B···O5^{ii}	0.96	2.57	3.510(19)	165

Symmetry codes: (i) 3-x,1/2+y,1-z; (ii) x,1+y,z; (iii) x,-1+y,z

Based on the experimental data, **1** is isostructural to $[Cu_2(nap)_4(DMSO)_2]$ [9] and is expected to be isostructural to $[Cu_2(nap)_4(H_2O)_2]$ [6].

Cu–$N_{3\text{-pic}}$ bond distances are 2.164(3) and 2.180(3) Å, slightly longer than $[Cu(bba)_2(3\text{-pic})_2]$ (1.999(2) Å) [38], [*cis*-Cu(p-hydroxybenzoate)$_2$(3-picoline)$_2$] (1.99(2) Å) [39], and $[Cu(2\text{-Cl-5-FC}_7H_3O_2)_2(3\text{-pic})_2(H_2O)_2]$ (2.009(4) Å) [40], where 2-Cl-5-$FC_7H_3O_2$ is 2-chloro-5-fluorobenzoate.

Cu–O_{nap} bond distances range from 1.935(3) to 2.029(3) Å, similar with a corresponding value in $[Cu(nap)_2(bipy)]H_2O$ (1.9435(16)−2.5810(16) Å) [6], $[Cu(nap)_2(phen)]H_2O$ (1.943(2)−2.577(2) Å) [6] and $[Cu(Nap)_2(3\text{-pym})_2]_n$ (1.9434(2)−1.9535(2) Å) [7], where bipy, phen, and 3-pym are 2,2′-bipyridine, 1,10-phenanthroline, and 3-pyridinemethanol, respectively.

3.2. *Crystal structure of 2*

The molecular structure of **2** is shown in figure 5, and selected bond distances and angles are listed in table 2. The complex is mononuclear and Cu(II) ion is square pyramidal,

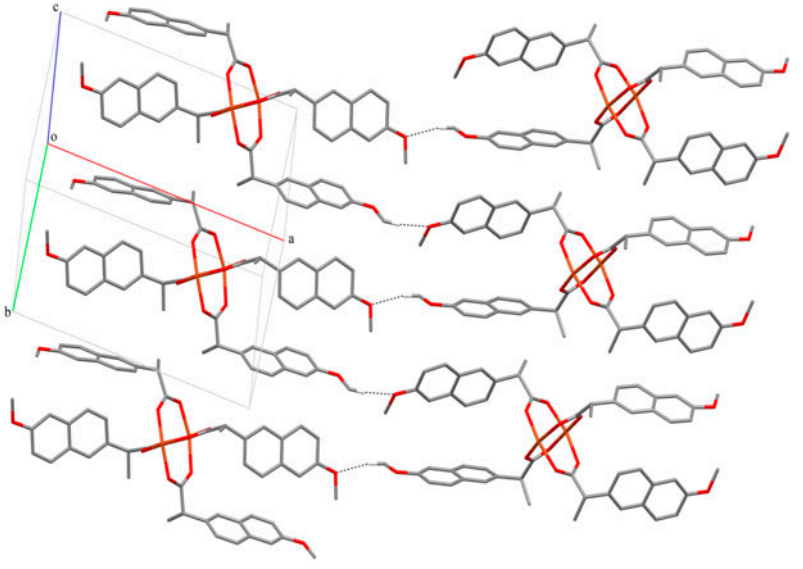

Figure 4. A crystal packing diagram of **1**.

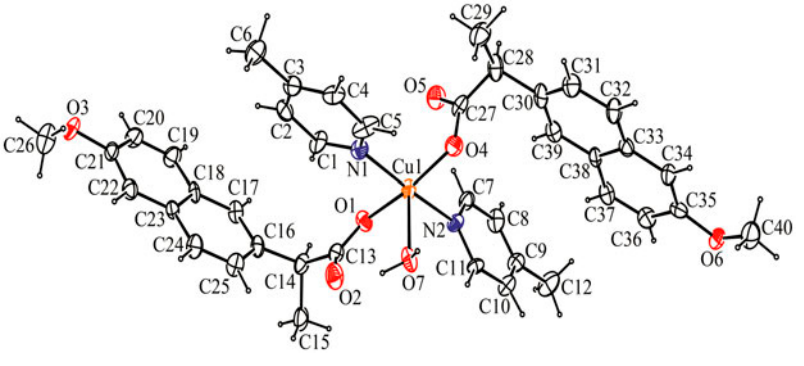

Figure 5. ORTEP III diagram and atom numbering scheme of **2**. Displacement ellipsoids are drawn at the 20% probability level.

coordinated to two oxygens of a pair of monodentate nap anions, two nitrogens from pyridine from a pair of neutral 4-pic, and one oxygen of water. The structural distortion index tau (τ) was calculated as 0.13 and the τ-value is suitable of square pyramidal.

Intramolecular O7–HB···O2 hydrogen bond between O–H of water and carboxyl oxygen of nap occurs. Adjacent complex units are connected via intermolecular O7–H7A···O1 ((i): $x, y+1, z$) hydrogen bonds between O–H group of the aqua ligand and carboxyl oxygen of nap, C7–H7···O4 ((ii): $x, y-1, z$) hydrogen bond between the phenyl group of 4-pic and carboxyl oxygen of nap, and C29–H29B···O5 ((i): $x, y+1, z$) hydrogen bond between the methoxy group of nap and the carboxyl oxygen of nap (figure 6; table 3).

Complex **2** is isostructural to $[Cu(nap)_2(py)_2(H_2O)]$ [8]. In $[Cu(nap)_2(py)_2(H_2O)]$, coordination geometry of copper(II) is square pyramidal. N(1) and N(2) of the two

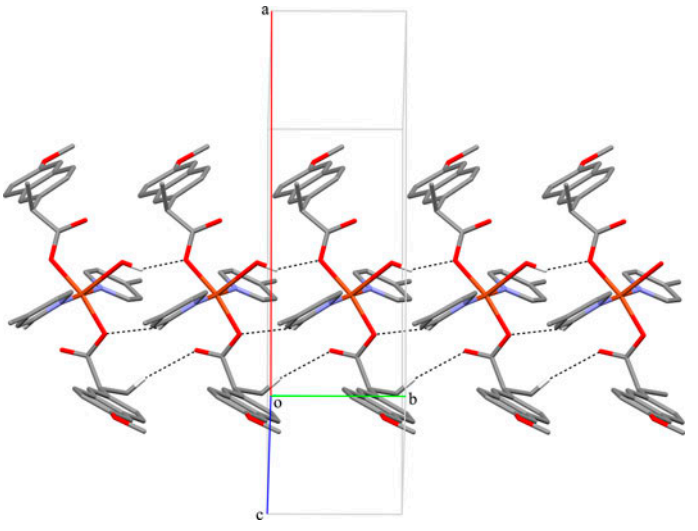

Figure 6. A crystal packing diagram of **2**.

pyridines and one carboxylate oxygen from each of the two nap ligands form the basal plane of a square pyramidal with a water at its apex.

$Cu–N_{4\text{-pic}}$ bond distances are 2.017(8)–2.062(9) Å, which are slightly longer than the corresponding in $[Cu(bba)_2(4\text{-pic})_2]$ (1.997(15) Å) [41], $[Cu(dipic)(4\text{-picoline})]_n$ (1.920(15) and 1.890(11) Å) [42], $[Cu(pmpa)(4\text{-methylpyridine})(H_2O)](H_2O)(ClO_4)$ (1.986(4) Å) [43], $[Cu(PEPA)(4\text{-methylpyridine})(H_2O)](ClO_4)$ (2.001(4) Å) [44], and $[CuBr(C_9H_{16}N_2Si)]_4$ (2.013 Å) [45]. But $Cu–N_{4\text{-pic}}$ bond distances are slightly shorter than in $[Cu_2(3\text{-}ClC_2H_4COO)(4\text{-pic})]$ (2.170(2) Å) [46] and where (H_2dipic), pmpa, PEPA, ($3\text{-}ClC_2H_4COO$), and ($C_9H_{16}N_2Si$) are pyridine-2,6-dicarboxylic acid, N-(2-picolyl)picolinamide, N-(2-pyridylethyl)picolinamide, 3-chloropropionato, and trimethylsilyl-(4-methylpyridine-2-yl)amin, respectively.

3.3. *FT-IR spectra*

The band assignments of naproxen and copper(II) nap complexes with 3-pic or 4-pic are listed in table 4. Examination of the FT-IR spectra of **1** demonstrated loss of carboxylic *ν*(OH) stretching (3490–2800 cm^{-1}) due to deprotonation of naproxen. A broad functional

Table 4. Selected IR spectral data[a] for the **Hnap** ligand, **1** and **2**.

	Hnap	**1**	**2**
υ_{COOH}(OH)	3250m	–	–
υ_{aqua}(OH)	–	–	3446sb
υ_{aro}(CH)	3003w	3062w	3064w
υ_{alf}(CH)	2975–2938w	2972–2936w	2986–2963w
υ(COOH)	1728	–	–
$\upsilon_{asym}(COO^-)$	–	1604s	1591s
$\upsilon_{sym}(COO^-)$	–	1398s	1380s

Notes: w, weak; m, medium; s, strong; vs, very strong; sb, strong broad.
[a]Frequencies in cm^{-1}.

group region indicates that water participated in coordination in **2**. The band at 3446 cm^{-1} corresponds to O–H stretching vibrations of water. The stretching peaks of both aromatic and aliphatic ν(CH) bonds of nap, 3-pic, and 4-pic are between 3062 and 2936 cm^{-1}. In the FT-IR spectrum of Hnap, the carbonyl of ν(COOH) at 1728 cm^{-1} disappeared in the corresponding metal complexs spectra. The FT-IR spectrums of **1** and **2** showed $\nu_{asym}(COO^-)$ at 1604 and 1591 cm^{-1}, $\nu_{sym}(COO^-)$ at 1398 and 1380 cm^{-1}. The positions of these frequencies and the separation between them, $\Delta\nu$ of 206 and 211 cm^{-1}, are in the range expected for bridging and monodentate carboxylate, respectively. Medium intensity band at 1214 cm^{-1} may be assigned to υ(C–O–C) asymmetric stretching while weak band at 1031 cm^{-1} is assigned to υ(C–O–C) symmetric stretch of nap. The band under 600 cm^{-1} in the complexes may be attributed to metal–oxygen and metal–nitrogen stretches.

3.4. *Thermal analysis*

The thermal behavior of **1** was followed to 900 °C in static air, showing decomposition in two steps. The first from 30–177 °C corresponds to the removal of two coordinated 3-pic with the endothermic DTA signal at 161 °C (DTG_{max} 161 °C). The observed mass loss of 13.00% agrees with the calculated mass loss of 15.12%. Degradation of four nap ligands take place in the second step (177–455 °C, DTG_{max} 248, 375 °C, DTA 243, 280, and 375 °C) with a mass loss of 74.00% (calcd 74.84%). The total observed mass loss of 87.00% agrees well with the calculated mass loss of 89.96% and the final decomposition product, CuO, was identified by PXRD with comparison of corresponding spectra obtained under the same conditions for the pure oxide.

Thermal decomposition of **2** occurs in two steps. The first at 30–173 °C is assigned to the loss of one water and two 4-pic ligands with a mass loss of 27.00% and a calculated value of 28.08%. An endothermic peak occurs in DTA at 122 °C (DTG_{max} 122, 146 °C). The second step between 173 and 461 °C corresponds to the loss of two nap ligands, representing a mass loss of 63.01% with a calculated value of 63.40%. (DTG_{max} 267, 534 °C). The final thermal product, CuO, was identified by PXRD (the total observed mass loss of 90.01%, calculated mass loss of 91.48%). The main diffraction peaks of final solid products are at 32.50, 35.55, 38.58, and 48.92(2θ) with distances of 2.76, 2.53, 2.33, and 1.86 Å, respectively, in agreement with the XRPD data of pure CuO.

3.5. *Catechol oxidase activity*

To gain deeper insight into the various parameters that determine copper-mediated substrate oxidations and bimetallic reactivity both in natural metalloenzymes and in synthetic analogs, quite a number of mono and dinuclear copper(II) complexes have been investigated as biomimetic catalysts for catechol oxidation [47–53]. Among the different catechols used in catechol oxidase model studies, $DTBCH_2$ is the most widely used substrate due to its low redox potential for the quinone–catechol couple, which facilitates its oxidation to the corresponding quinone (3,5-DTBQ), and to the presence of bulky substituents, that slow further oxidation reactions such as ring opening [54–56]. The two-electron oxidation of $DTBCH_2$ to quinone was investigated since this is the reaction that the copper-containing enzyme catechol oxidase catalyzes. There are a number of factors that need to be considered, such as electrochemical properties, the geometry imposed by the ligands on the metal, the nature of any exogenous donors, the basicity of the donor, and steric features of the ligands [17, 57].

To compare the difference between mononuclear and dinuclear complexes, we have studied our copper complexes for catecholase activity, using the changes in the electronic spectrum after the addition of $DTBCH_2$ substrate [57].

The catalytic oxidation of $DTBCH_2$ shows that both dinuclear **1** and mononuclear **2** showed catechol oxidase activity at room temperature in methanol. The experimental studies showed that dinuclear complexes have better activity than mononuclear complexes because this mechanism requires two metal ions in close proximity [58]. The Cu···Cu distance in dinuclear copper complexes needs to be less than 5 Å [17, 18] for effective electron transfer during the catalytic process to exhibit catecholase activity. In our study, the Cu···Cu distance is 2.69 Å. Time-dependent increase in quinone absorbance is displayed in figure 7. In that study, 10^{-4} M complex and 4×10^{-3} M substrate were stirred at equal volumes and quinone formation was determined by UV–vis spectrophotometer at 395 nm.

The kinetic study was performed by the initial rate method by monitoring the absorption at 395 nm for the first 1 min. Constant concentration of complex and different concentration of substrate were prepared (complex: 10^{-4} M, substrate: 5–10–15–20–30–40–50 $\times 10^{-4}$ M). At low concentrations of $DTBCH_2$, a first-order dependence of the substrate concentration was observed and saturation kinetics were found at high substrate concentrations [56, 59]. The kinetic parameters (table 5) were determined by using the Michaelis–Menten equation (figure 8) and a Lineweaver–Burk plot (figure 9).

The turnover number for catechol oxidase enzyme is $8.255 \times 10^6\ h^{-1}$. Both dinuclear and mononuclear copper(II) complexes displayed much less turnover number, but these results are quite comparable to those reported [56, 57, 60–63].

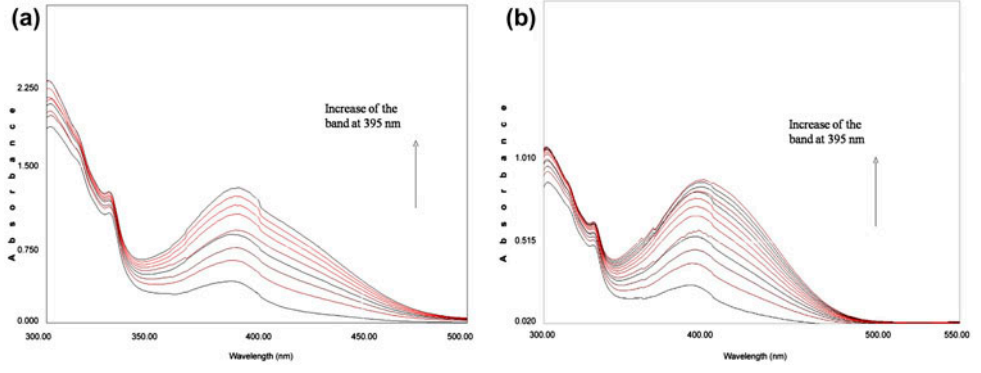

Figure 7. UV–Vis spectra (300–550 nm) of **1** (a) and **2** (b) (1×10^{-4} M in CH_3OH); $DTBCH_2$ (4×10^{-3} M in CH_3OH).

Table 5. K_m, V_{max}, and k_{cat} values for complexes.

	V_{max} (Ms^{-1})	K_m (M)	k_{cat} (h^{-1})
$[Cu_2(\mu\text{-nap})_4(3\text{-pic})_2]$	4.26×10^{-6}	1.45×10^{-4}	153.36
$[Cu(nap)_2(H_2O)(4\text{-pic})_2]$	2.24×10^{-6}	1.1×10^{-4}	80.64

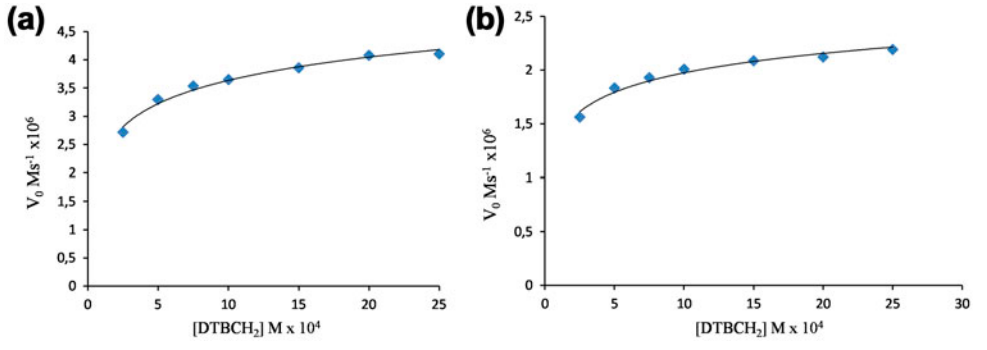

Figure 8. Dependence of the reaction rates on the $DTBCH_2$ concentrations for the oxidation reaction catalyzed by **1** (a) and **2** (b). The reaction was performed in methanol at room temperature.

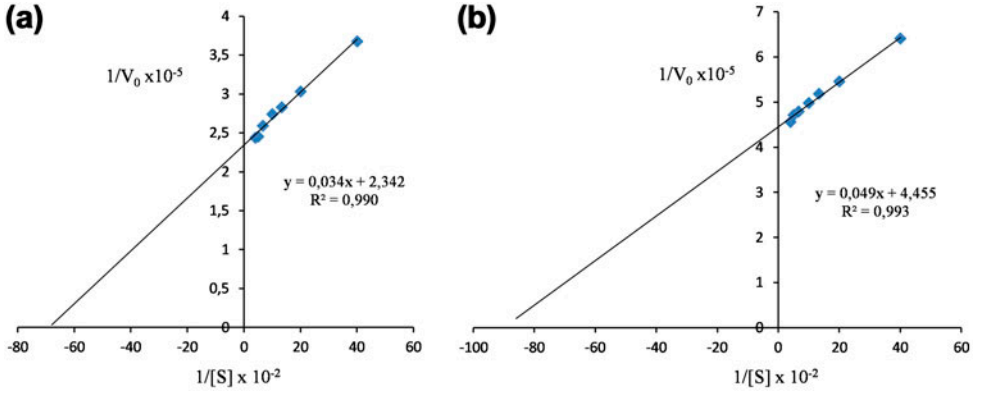

Figure 9. Lineweaver–Burk plot for catalysis by **1** (a) and **2** (b).

Table 6. Antimicrobial activities of the compounds evaluated by MIC (μg mL^{-1}).

Compounds	*E. feacalis*	*C. albicans*
$[Cu_2(\mu\text{-nap})_4(3\text{-pic})_2]$	256	128
$[Cu(nap)_2(H_2O)(4\text{-pic})_2]$	256	128
Naproxen	512	256
$CuSO_4$	>1024	>1024
3-Picoline	512	256
4-Picoline	512	256
DMSO	512	256
Vancomycine	2	–
Amphotericine B	–	0.0625

3.6. *Antimicrobial activity*

The *in vitro* antimicrobial properties of the compounds against Gram-positive bacteria and yeast are presented in table 6. Among the tested micro-organisms, *E. faecalis* and

C. albicans appear to be the most sensitive strains with MIC values of 256 and 128 μg mL^{-1}, respectively. However, $[Cu_2(\mu\text{-nap})_4(3\text{-pic})_2]$ and $[Cu(nap)_2(H_2O)(4\text{-pic})_2]$ were inactive against the other micro-organisms (MIC values > 512 μg mL^{-1}). One strain of yeast *C. albicans* (ATCC 10231) was more sensitive than the others. Antimicrobial activities of the complexes were higher than the drug molecules in the absence of copper. These results have good agreement with similar studies available in the literature [64–67].

4. Conclusions

Two copper(II) naproxenato complexes with 3-pic and 4-pic have been synthesized and characterized by elemental analyses, FT-IR, thermal analyses, and X-ray diffraction. X-ray crystal structure analysis demonstrated that **1** is dinuclear and **2** is mononuclear. The complexes have square-pyramidal geometry. Nap ligands bridge in **1** and are monodentate in **2**. Thermal stability of **1** and **2** are up to 161 and 122 °C, respectively, before the onset of decomposition. Catechol oxidase activities of **1** and **2** using $DTBCH_2$ as substrate in methanol showed good catechol oxidase activity. Biological assays showed antimicrobial activity of the complexes against *C. albicans* and *E. faecalis*.

Supplementary material

Supplementary data CCDC-946001 and CCDC-946002 contain the supplementary crystallographic data for **1** and **2**, respectively. These data can be obtained free of charge via http://www.ccdc.cam.ac.uk/conts/retrieving.html, or from the Cambridge Crystallographic Data Center, 12 Union Road, Cambridge CB2 1EZ, UK; Fax: (+44) 1223 336 033; or E-mail: deposit@ccdc.cam.ac.uk.

Acknowledgement

This work was financially supported by the Erzincan University under project no. 110205.

References

[1] K. Kim, J. Yoon, J.K. Kim, S.J. Baek, T.E. Eling, W.J. Lee, J. Ryu, J.G. Lee, J. Lee, J. Yoo. *Biochem. Biophys. Res. Commun.*, **325**, 1298 (2004).
[2] G. Ribeiro, M. Benadiba, A. Colquhoun, D. de Oliveira Silva. *Polyhedron*, **27**, 1131 (2008).
[3] R.N. Brogden, R.C. Heel, G.E. Pakes, T.M. Speight, G.S. Avery. *Drugs*, **20**, 24 (1980).
[4] J.C. Boylan, J. Cooper, Z.T. Chowhan. *Handbook of Pharmaceutical Excipients*, American Pharmaceutical Association, Washington, DC (1986).
[5] J.E. Weder, C.T. Dillon, T.W. Hambley, B.J. Kennedy, P.A. Lay, J.R. Biffin, H.L. Regtop, N.M. Davies. *Coord. Chem. Rev.*, **232**, 95 (2002).
[6] F. Dimiza, F. Perdih, V. Tangoulis, I. Turel, D.P. Kessissoglou, G. Psomas. *J. Inorg. Biochem.*, **105**, 476 (2011).
[7] A.L. Abuhijleh, J. Khalaf. *Eur. J. Med. Chem.*, **45**, 3811 (2010).
[8] C. Dendrinou-Samara, P.D. Jannakoudakis, D.P. Kessissoglou, G.E. Manoussakis, D. Mentzafos, A. Terzis. *J. Chem. Soc., Dalton Trans.*, 3259 (1992).

[9] C. Dendrinou-Samara, D.P. Kessissoglou, G.E. Manoussakis, D. Mentzafos, A. Terzis. *J. Chem. Soc., Dalton Trans.*, 959 (1990).
[10] F. Dimiza, A.N. Papadopoulos, V. Tangoulis, V. Psycharis, C.P. Raptopoulou, D.P. Kessissoglou, G. Psomas. *J. Inorg. Biochem.*, **107**, 54 (2012).
[11] J. Sharma, A.K. Singla, S. Dhawan. *Int. J. Pharm.*, **260**, 217 (2003).
[12] C. Dendrinou-Samara, G. Tsotsou, L.V. Ekateriniadov, A. Kortsaris, C.P. Raptopoulou, A. Terzis, D. Kyriakidis, D.P. Kessissoglou. *J. Inorg. Biochem.*, **71**, 171 (1998).
[13] J.R.J. Sorenson. *Prog. Med. Chem.*, **26**, 437 (1989).
[14] A.C. Rosenzweig, M.H. Sazinsky. *Curr. Opin. Struct. Biol.*, **16**, 729 (2006).
[15] L.M. Mirica, X. Ottenwaelder, T.D.P. Stack. *Chem. Rev.*, **104**, 1013 (2004).
[16] N. Oishi, Y. Nishida, K. Ida, S. Kida. *Bull. Chem. Soc. Jpn.*, **53**, 2847 (1980).
[17] M.R. Malachowski, H.B. Huynh, L.J. Tomlinson, R.S. Kelly, J.W. Furbee. *J. Chem. Soc., Dalton Trans.*, 31 (1995).
[18] R. Than, A.A. Feldman, B. Krebs. *Coord. Chem. Rev.*, **182**, 211 (1999).
[19] S. Torelli, C. Belle, I. Gautier-Luneau, J.L. Pierre, E. Saint-Aman, J.M. Latour, L. Le Pape, D. Luneau. *Inorg. Chem.*, **39**, 3526 (2000).
[20] C. Belle, C. Beguin, I. Gautier-Luneau, S. Hamman, C. Philouze, J.L. Pierre, F. Thomas, S. Torelli, E. Saint-Aman, M. Bonin. *Inorg. Chem.*, **41**, 479 (2002).
[21] G. Speier. *J. Mol. Catal.*, **37**, 259 (1986).
[22] J.P. Chyn, F.L. Urbach. *Inorg. Chim. Acta*, **189**, 157 (1991).
[23] J. Balla, T. Kiss, R.F. Jameson. *Inorg. Chem.*, **31**, 58 (1992).
[24] K. Selmeczi, M. Reglier, M. Giorgi, G. Speier. *Coord. Chem. Rev.*, **245**, 191 (2003).
[25] E. Monzani, L. Quinti, A. Perotti, L. Casella, M. Gullotti, L. Randaccio, S. Geremia, G. Nardin, P. Faleschini. G. Tabbı`, *Inorg. Chem.*, **37**, 553 (1998).
[26] E. Monzani, G. Battaini, A. Perotti, L. Casella, M. Gullotti, L. Santagostini, G. Nardin, L. Randaccio, S. Geremia, P. Zanello, G. Opromolla. *Inorg. Chem.*, **38**, 5359 (1999).
[27] A.L. Hughes. *Immunogenetics*, **49**, 106 (1999).
[28] D. Meiwes, B. Ross, M. Kiesshauer, K. Cammann, H. Witzel, M. Knoll, M. Borchardt, C. Sandermaier. *Lab. Med.*, **15**, 24 (1992).
[29] G. Grigoropoulou, K.C. Christoforidis, M. Louloudi, Y. Deligiannakis. *Langmuir*, **23**, 10407 (2007).
[30] M.K. Panda, M.M. Shaikh, R.J. Butcher, P. Ghosh. *Inorg. Chim. Acta*, **372**, 145 (2011).
[31] Z.-F. Chen, Z.-R. Liao, D.-F. Li, W.-K. Li, X.-G. Meng. *J. Inorg. Biochem.*, **98**, 1315 (2004).
[32] T. Klabunde, C. Eicken, J.C. Sacchettini, B. Krebs. *Nat. Struct. Biol.*, **5**, 1084 (1998).
[33] G.M. Sheldrick, *SHELXS97 and SHELXL9*, University of Göttingen, Germany (1997).
[34] Stoe & Cie, X-Area (Version 1.18) and X-Red32 (Version 1.04), Darmstadt, Germany (2002).
[35] Clinical and Laboratory Standards Institute (CLSI), *Methods of Dilution Antimicrobial Susceptibility Tests for Bacteria that Grow Aerobically, Approved Standard*, 7th Edn, CLSI, Wayne (2006).
[36] National Committee for Clinical Laboratory Standards Institute. *Reference Method for Broth Dilution Antifungal Susceptibility Testing of Yeasts. Approved Standard*, 2nd Edn, NCCLS document M27–A2, NCCLS, Wayne, PA (2002).
[37] A.W. Addison, T.N. Rao, J. Reedijk, J. van Rijn, G.C. Verschoor. *J. Chem. Soc., Dalton Trans.*, 1349 (1984).
[38] S. Caglar, Z. Heren, O. Büyükgüngör. *J. Coord. Chem.*, **64**, 2706 (2011).
[39] R.P. Sharma, A. Singh, A. Saini, P. Venugopalan, A. Molinari. *J. Mol. Struct.*, **888**, 291 (2009).
[40] R.P. Sharma, A. Saini, S. Singh, A. Singh, P. Venugoplan, P. Starynowicz, J. Jezierska. *J. Mol. Struct.*, **1006**, 672 (2011).
[41] S. Caglar, S. Demir. *J. Chem. Crystallogr.*, **42**, 464 (2012).
[42] Z.A. Sıddıqı, M. Khalid, S. Kumar, M. Shahid. *X-ray Struct. Anal. Online*, **25**, 71 (2009).
[43] C.-Y. Wu, C.-C. Su. *Polyhedron*, **16**, 383 (1997).
[44] C.-Y. Wu, C.-C. Su. *Polyhedron*, **16**, 2465 (1997).
[45] K. Smolander, M. Malik. *Acta Chem. Scand.*, **38**, 619 (1984).
[46] G. Glatz, R. Kempe. *Z. Kristallogr. NCS*, **223**, 311 (2008).
[47] I.A. Koval, D. Pursche, A.F. Stassen, P. Gamez, B. Krebs, J. Reedijk. *Eur. J. Inorg. Chem.*, **9**, 1669 (2003).
[48] C.-H. Kao, H.-H. Wie, Y.-H. Liu, G.-H. Lee, Y. Wang, C.-J. Lee. *J. Inorg. Biochem.*, **84**, 171 (2001).
[49] J. Rall, M. Wanner, M. Albrecht, F.M. Hornung, W. Kaim. *Chem. Eur. J.*, **5**, 2802 (1999).
[50] C. Eicken, B. Krebs, J.C. Sacchettini. *Curr. Opin. Struct. Biol.*, **9**, 677 (1999).
[51] G. Battaini, E. Monzani, L. Casella, L. Santagostini, R. Pagliarin. *J. Biol. Inorg. Chem.*, **5**, 262 (2000).
[52] M.R. Malachowski, J. Carden, M.G. Davidson, W.L. Driessen, J. Reedijk. *Inorg. Chim. Acta*, **257**, 59 (1997).
[53] B. Sreenivasulu, F. Zhao, S. Gao, J.J. Vittal. *Eur. J. Inorg. Chem.*, **13**, 2656 (2006).
[54] J. Reim, B. Krebs. *J. Chem. Soc., Dalton Trans.*, 3793 (1997).
[55] R. Wegner, M. Gottschaldt, H. Gorls, E.G. Jager, D. Klemm. *Chem. Eur. J.*, **7**, 2143 (2001).
[56] D. Sadhukhan, A. Ray, R.J. Butcher, C.J. Gomez Garcia, B. Dede, S. Mitra. *Inorg. Chim. Acta*, **376**, 245 (2011).

[57] C. Fernandes, A. Neves, A.J. Bortoluzzi, A.S. Mangrich, E. Rentschler, B. Szpoganicz, E. Schwingel. *Inorg. Chim. Acta*, **320**, 12 (2001).
[58] Abd E.-M.M. Ramadan, M.M. Ibrahim, I.M. El-Mehasseb. *J. Coord. Chem.*, **65**, 2256 (2012).
[59] S. Caglar, E. Adiguzel, B. Caglar, T. Saykal, E. Sahin, O. Buyukgungor. *Inorg. Chim. Acta*, **397**, 101 (2013).
[60] J. Mukherjee, R. Mukherjee. *Inorg. Chim. Acta*, **337**, 429 (2002).
[61] S.-C. Cheng, H.-H. Wei. *Inorg. Chim. Acta*, **340**, 105 (2002).
[62] A.C.D. Midoes, P.E. Aranha, M.P. dos Santos, E. Tozzo, S. Romera, R.H.A. Santos, E.R. Dockal. *Polyhedron*, **27**, 59 (2008).
[63] A.I. Hanafy, Z.M. El-Bahy, I.O. Ali. *J. Coord. Chem.*, **65**, 1459 (2012).
[64] S. Thalamuthu, B. Annaraj, S. Vasudevan, S. Sengupta, M.A. Neelakantan. *J. Coord. Chem.*, **66**, 1805 (2013).
[65] A.M. Mansour. *J. Coord. Chem.*, **66**, 1118 (2013).
[66] V.K. Chityala, K.S. Kumar, N.J.P. Subhashini, P. Raghavaiah, Shivaraj. *J. Coord. Chem.*, **66**, 274 (2013).
[67] H. Keypour, M. Shayesteh, R. Golbedaghi, A. Chehregani, A.G. Blackman. *J. Coord. Chem.*, **65**, 1004 (2012).